3. Materials and experimentation methodology.

The chapter provides the details of coating preparation and experimental procedures used in the present work. Furthermore, the various analytical techniques and instrument details employed to analyze nanoparticles, coatings, and worn surfaces are also described.

3.1. Materials.

3.1.1. Sample preparation for various coatings.

As discussed in the previous chapter, three different coatings are explored in the present study. These coatings were done on different samples prepared from various materials. The multilayer Ti/TiN coatings were deposited on 25.4 mm diameter and 8 mm thick cylindrical discs machined from a 100Cr6 cylindrical rod of 30 mm diameter. 10 mm thick discs were machined from the cylindrical rods, which were then grounded to 8 mm. Mo/DLC multilayer coatings were deposited on galling samples prepared as per ASTM G196 [7]. The samples were prepared from 16 mm hexagonal SS 304 rods in a CNC lathe machine. The samples for PU-based coatings were prepared on 100Cr6 plates of 25X25X5 mm in dimension. The samples were machined from a rectangular plate. All the samples were grounded and polished to the required roughness before deposition of the coating.

3.1.2. Synthesis of MoS_2 and MoS_2-ODT nanosheets.

MoS_2 nanosheets were prepared hydrothermally reducing sodium molybdate with thiourea [213]. In this case, a 35 percent aqueous solution of HCl was added while stirring continuously for 30 minutes at 90˚C to a 10 mL aqueous solution of sodium molybdate and hydroxylamine hydrochloride. The reaction solution was then gradually supplemented with 0.78 g thiourea while being agitated for an additional 15 minutes. The MoS_2 reaction precursors were placed

in a Teflon-lined stainless steel autoclave and kept in a regular hot air oven at 230˚C for 24 hours. The hydrothermal reduction process converted the reaction precursors' solution phase into the segregated black-colored MoS_2 product. The MoS_2 was centrifuged at 5000 rpm and repeatedly rinsed with distilled water until the pH of the water was almost 7. The MoS_2 nanosheets were separated by filtration and dried at 90˚C in a regular hot air oven. To prepare the dried MoS_2 nanosheets for further use and characterization, they were crushed into a fine powder using a mortar and pestle.

MoS_2 nanosheets agglomerate when van der Waals forces cause the dangling sulphur atoms in the MoS_2 lamella to interact cohesively. One possible way to prevent the agglomeration of nanosheets is to chemically functionalize them with surface-active molecules. A lengthy alkyl chain was used to functionalize the MoS_2 nanosheets. **Figure 3.1** provides a schematic representation of the functionalization of MoS_2 nanosheets by ODT molecules. In this case, the ODT solution was made by mixing 0.6 g of 1-octadecanethiol (ODT) with 50 mL of methanol. The MoS2 nanosheets (0.11 g) were distributed throughout the ODT solution using ultrasound energy. The reaction mixture was sonicated using a bath sonicator. The final step was drying the functionalized MoS_2 nanosheets in a typical hot air oven at 90˚C. For further use and characterization, the dried MoS_2-ODT nanosheets were crushed into a fine powder using a mortar and pestle.

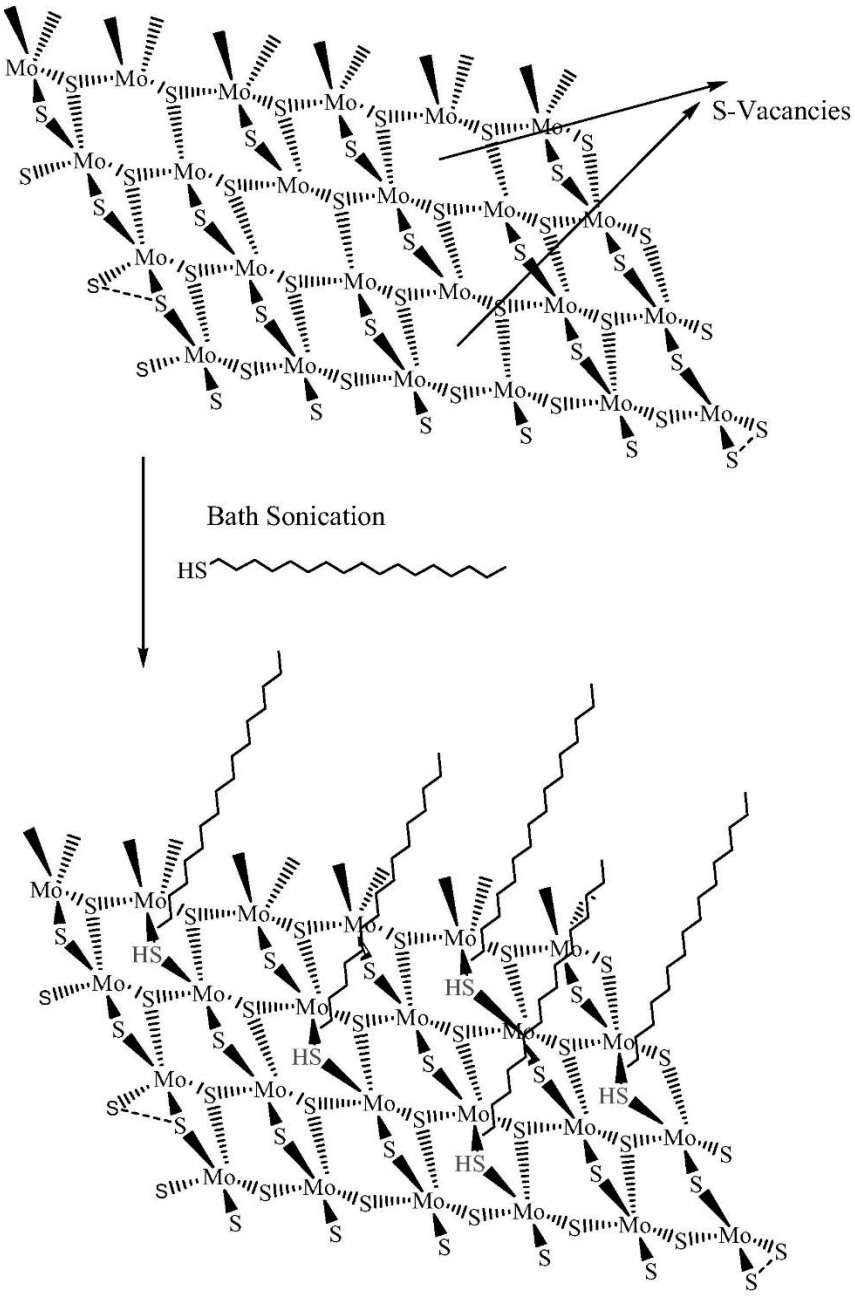

Figure 3.1. Schematic representation of MoS2 nanosheets functionalized with ODT. Reprinted with permission from reference [3].

3.2. Coating systems.

The multilayer Ti/TiN coatings and Mo/DLC coatings were prepared through the PVD technique. At the same time, the soft PU-based coatings were prepared by air spray technique.

The different systems and their specifications used for coatings, as mentioned earlier, are discussed below:

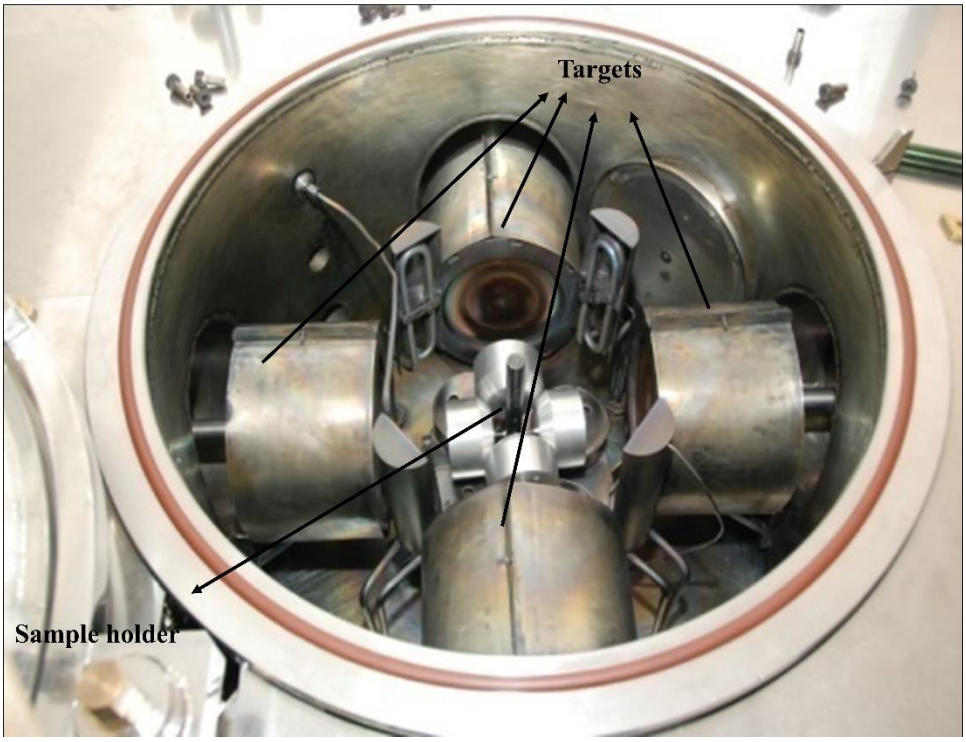

Figure 3.2. Semi-industrial sputtering system.

3.2.1. Semi-industrial sputtering system.

Figure 3.2 shows the semi-industrial sputtering system. The system is equipped with 4 targets of 6 inches. The substrates to be coated are placed on holders attached to the motorized planetary gear arrangement. The system is capable of holding a large number of targets due to its high working volume of 272 litres. The targets were powered by a pulsed DC power source capable of operating at 5KW. Due to the size of the sputtering system, unbalanced magnetrons were used for the proper formation of the plasma. The gas inflow in the system was controlled through a four channel mass flow controller, which can even be programmed to purge gas into the chamber at regular intervals for the deposition of multilayer structures of nitrides and carbides of transition metals. The programmable mass flow controller can also be used to deposit graded coatings by controlling the amount of gas inflow into the chamber. Since the

PVD works under high vacuum conditions, the sputtering system was equipped with rotary and turbomolecular vacuum pumps. The rotary pump was used to create the vacuum up to 10^{-3} mbar; after that turbomolecular pump was used to attain a vacuum in the range of 10^{-6} mbar. All the valves were pneumatically controlled, and all the magnetrons were water cooled with water circulating inside the system from a chiller at 18˚C. A bias voltage generator capable of operating at -2000 V was also attached to the substrate holders for argon etching and better flow of ions during the deposition process. A substrate heater could operate in the temperature range of 0 - 1000˚C to assist high-temperature coating deposition.

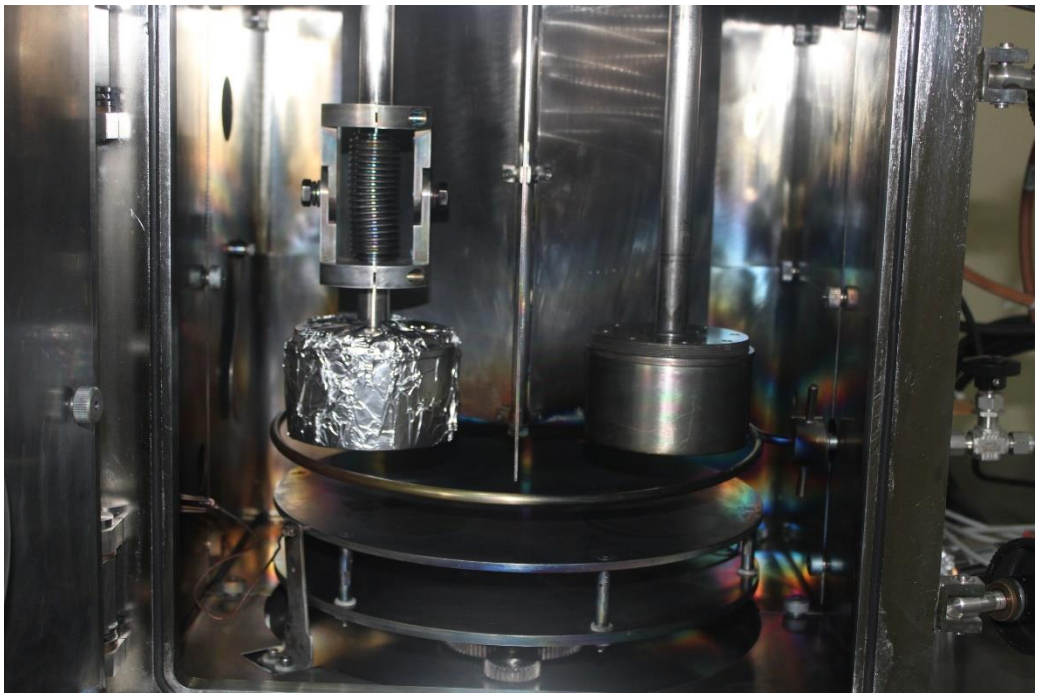

Figure 3.3. Laboratory scale balanced sputtering system.

3.2.2. Laboratory scale balanced sputtering system.

Figure 3.3 shows the laboratory scale balanced sputtering system, equipped with two balanced magnetrons capable of holding targets of 3 inches. The substrate holder is a rotating table with magnetrons on top of it. This system was equipped with rotary and turbomolecular pumps to attain a high vacuum. However, the targets were powered by pulsed DC and HIPIMS power sources. The HIPIMS power source can operate at a maximum power of 6 kW. The bias voltage

generator was capable of operating at -1000 V. The gas flow inside the vacuum chamber was controlled by two channel mass flow controllers. The targets were water-cooled like the semi-industrial system, but the temperature of the cooled water was kept lower because of the excessive heating of the target from the HIPIMS power source.

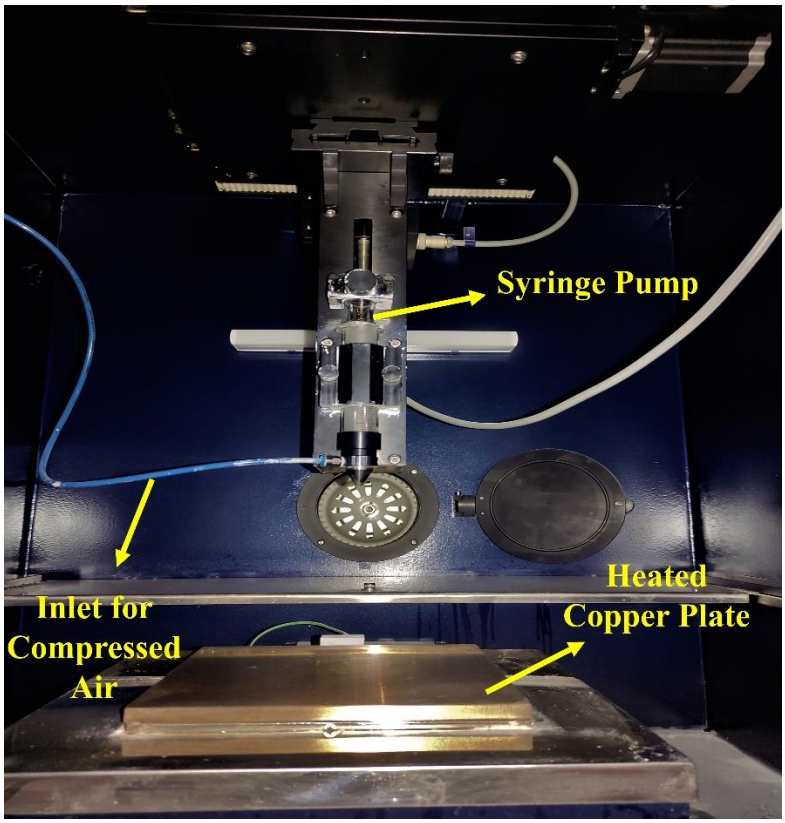

Figure 3.4. Spray Pyrolysis Equipment.

3.2.3. Spray pyrolysis equipment.

The spray pyrolysis equipment shown in **Figure 3.4** was used to coat PU-based coatings. The coating solution was atomized into small droplets by passing compressed air and solution through a nozzle. The atomized droplets were then sprayed on the samples. The dispensing rate of solution and the speed of the spray head were computer controlled. The substrate holder was a heated copper plate of 150 X 150 mm in dimension, capable of operating up to 500˚C. The dispensing unit was attached to a stepper motor, which can dispense the solution at a rate of 1-

10 ml/min. The drive speed of the spray head on the X and Y axis ranged from 5-20 and 2-12 mm/sec, respectively.

3.3. Preparation of coatings.

All the three types of coatings discussed in the present study were created with the help of the coating instruments discussed above. However, many steps are involved before and during the coating process that must be taken care of.

3.3.1. PVD coatings.

Figure 3.5 represents the flowchart of the processes involved in a PVD coating process. During the substrate preparation stage, the substrates are grounded and polished to the required roughness and then cleaned thoroughly in acetone and isopropyl alcohol for 1 hour. After cleaning the substrates, they are loaded into the vacuum chamber. A rotary pump is used to create the initial vacuum of 10^{-3} mbar; after that turbomolecular pump is switched on to attain a high vacuum of 10^{-6} mbar. When the desired vacuum is reached, the mass flow controller is switched to allow argon gas to flow into the chamber. Bias cleaning of the substrate is done by applying a high bias voltage. The bias cleaning removes impurities and oxide layers formed on the surface of the substrates. After the bias cleaning, the targets are energized from their respective power sources, and the coating starts depositing on the surface of the substrates. When the coating is complete, the power sources and the vacuum pump is switched off, and the substrates are removed. The specific values of power and voltage used in the deposition process of Ti/TiN and Mo/DLC multilayer coatings can be found in the later chapters dedicated to these coatings.

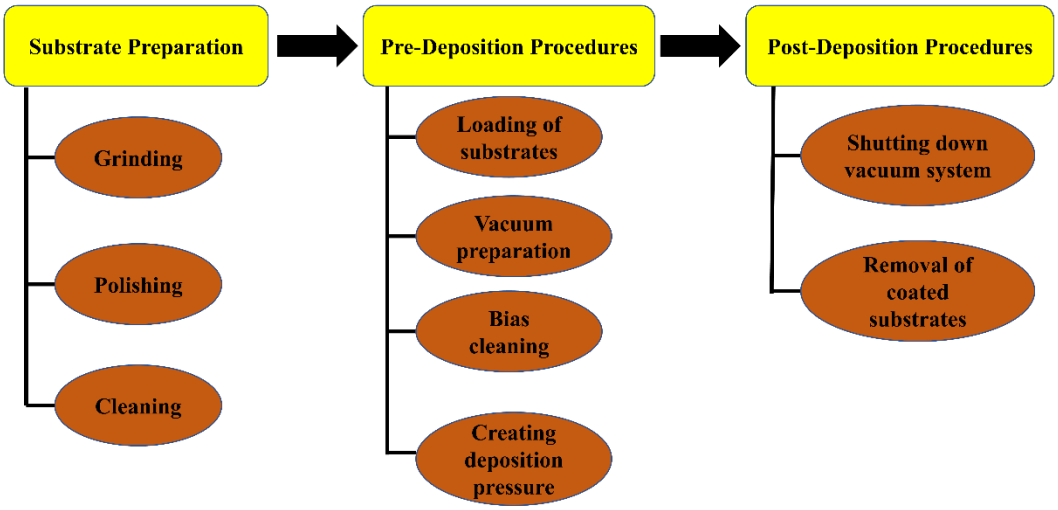

Figure 3.5. Flowchart of coating fabrication through PVD technique.

3.3.2. PU-based coatings.

The coating procedure of PU-based coatings with the help of spray pyrolysis equipment was relatively simple. The grounded substrates were cleaned ultrasonically in ethanol and isopropyl alcohol for 1 hour. After that, they were loaded into the spray pyrolysis chamber. A syringe containing the PU solution was attached to the computer-controlled syringe pump. The desired discharge speed of the syringe pump and the actuation speed of the coating arm was then fed to the computer to start the coating process.

3.4. Characterization of nanosheets.

3.4.1. Transmission electron microscopy (TEM).

The morphological and nanostructural features of MoS_2 and MoS_2–ODT nanosheets were examined using a high–resolution transmission electron microscope (TEM), JEM 2100, JEOL Ltd., (Japan). For sample preparation, the ethanolic dispersion of each nanosheet was drop–cast on a separate TEM grid (copper material, diameter–3 mm, thickness–100 μm, and 200

mesh lacey carbon). The operating voltage was kept constant at 300 kV, and a high vacuum in the range of 10^{-6} Torr was required to acquire the low–and high–resolution TEM images.

3.4.2. X-ray diffraction (XRD).

In comparison to visible light, the wavelength of X-ray electromagnetic waves is shorter. XRD spectroscopy is the most efficient technique to examine the crystalline structure and recognize the many phases of materials with the same composition. Because of crystallographic planes, X-ray beams impacting powder or thin film materials will diffract. Diffraction operates on the fundamental tenets of Bragg's Law. Bragg's equation calculated the interlamellar distance between parallel succeeding crystallographic planes.

$$n\lambda = 2\,d\sin\theta \qquad \text{Eq (3.1)}$$

Where n is an integer; λ is the wavelength of incident X-ray radiation; d is interlamellar spacing between parallel successive crystallographic planes; Θ is the incident angle.

The crystalline features of MoS_2 and MoS_2–ODT nanosheets were analyzed by X-ray diffractometer (XRD), Rigaku Miniflex 600 D/teX Ultra using Cu Kα line as an X-ray radiation source. The wavelength (λ) of the radiation was 0.15418 nm. The typical voltage and current were kept constant at 40 kV and 15 mA, respectively. The XRD patterns of MoS_2 and MoS_2–ODT samples were collected in the 2Θ range of 10 to 80° with the grazing angle of 2˚.

The crystalline structure of Ti/TiN multilayer coating was also studied with the same XRD, but the grazing angle was lowered down to 0.5˚.

3.4.3. Fourier transform infrared spectroscopy (FTIR).

FTIR spectroscopy was utilised to collect an infrared spectrum of transmission or absorption to investigate the numerous functional groups in solid, liquid, and gaseous materials. MoS_2 and MoS_2-ODT nanosheets were independently crushed into pellets with KBr (dry) powder to get

their FTIR spectra. Thermo-Scientific Nicolet 8700 spectrometer was used to get the transmittance FTIR spectra of MoS_2 and MoS_2-ODT at a resolution of 4 cm^{-1} in the spectral range between 400 and 4000 cm^{-1}. It was used to affirm the formulation and chemical functionalization of nanosheets.

3.5. Characterization of coatings.

3.5.1. Field emission scanning microscopy (FESEM).

FESEM is an advanced version of the scanning electron microscope. It produces a thousand times better image than any conventional SEM. The ultra-high vacuum chamber uses a Schottky field emitter. The ultra-high vacuum system is supported by two ion pumps and one turbomolecular pump. It has a resolution of 1 nm at 20 kVA. Supra 40 VP (Carl Zeiss), FESEM was used to study the cross-sectional morphology of the coatings, the wear scars, and to ascertain the thickness of the deposited coating.

3.5.2. Nanoindentation hardness tester.

The thin film coatings' mechanical properties like hardness, elastic modulus, and fracture toughness can be evaluated by a nanoindentation hardness tester. The mechanical properties are calculated by combining the data of the loading and unloading cycle with the displacement of the indenter. The software's working is based on the empirical equations and relationships created by Oliver and Pharr [214]. The CSM instrument, nanoindentation hardness tester with a load range from 0.5 to 300 nN, and the resolution of 0.04 μN and 0.3 nm in terms of load and depth, respectively, was used to calculate the hardness and elastic modulus of the coatings.

3.5.3. Micro Raman spectrometer.

Raman spectroscopy can be used to analyze the chemical phases of solid and liquid samples. A micro Raman spectrometer can be used to measure the vibrational spectra of the solid samples. The detector collects the light scattered by the molecules. A typical Raman spectrum

comprises of several peaks, indicating the wavelength position and intensity of the Raman scattered light. HORIBA Jobin Yvon, a Raman spectrometer, was used to analyze the bonding in Ti/TiN and Mo/DLC multilayer coatings. The spectrometer consists of a 15 mW powered laser with an air-cooled 1024X256 pixels CCD detector. The instrument was clubbed with a confocal microscope system to pinpoint the location for Raman spectroscopy measurements.

3.5.4. X-Ray photoelectron spectroscopy (XPS).

XPS, a quantitative spectroscopic technique, is used to probe the chemical composition of specimens. The X-ray photoelectrons are characteristic electrons ejected from the uppermost atomic layer of samples when an atom absorbs an X-ray photon. The electron emitted from the electron shell of an atom exhibits characteristics energy levels, unveiling the composition of chemical elements in the sample being examined. Therefore, the XPS technique is referred to as a surface chemical analysis. The XPS operates under ultra-high vacuum (10^{-9} bar). The chemical composition of the tribo–film developed on the worn surface was examined by XPS (Thermoscientific, K–Alpha) using Al Kα radiation X-ray source. The binding energies of all spectra were calibrated with the C 1s and binding energy of 284.5 eV.

3.6. Tribological testing.

Two types of tribological testing were done in the present study, reciprocating and galling. For reciprocating testing, different tribometers were used for three different coatings. While for galling tests, a tribometer developed by Harsha et al. [8] as per ASTM G196 was used.

3.6.1. TKLB tribometer (Ball on disc tribometer).

This reciprocating tribometer is used for ambient and elevated temperature testing Ti/TiN multilayer coating. **Figure 3.6** shows the details of the TKLB tribometer used for reciprocating tests. The tribometer was enclosed in Plexiglas to maintain the same humidity across all tests. The coated discs were placed on the reciprocating table, whose movement was controlled by a

frequency-controlled DC motor with an eccentric adjustment. The tribometer can apply load in the range of 0-50 N. The frequency and stroke length of the reciprocating table ranged from 0-50 Hz and 0-3 mm, respectively. The tribometer also has a heater attached to the table, capable of raising temperature till 250˚C.

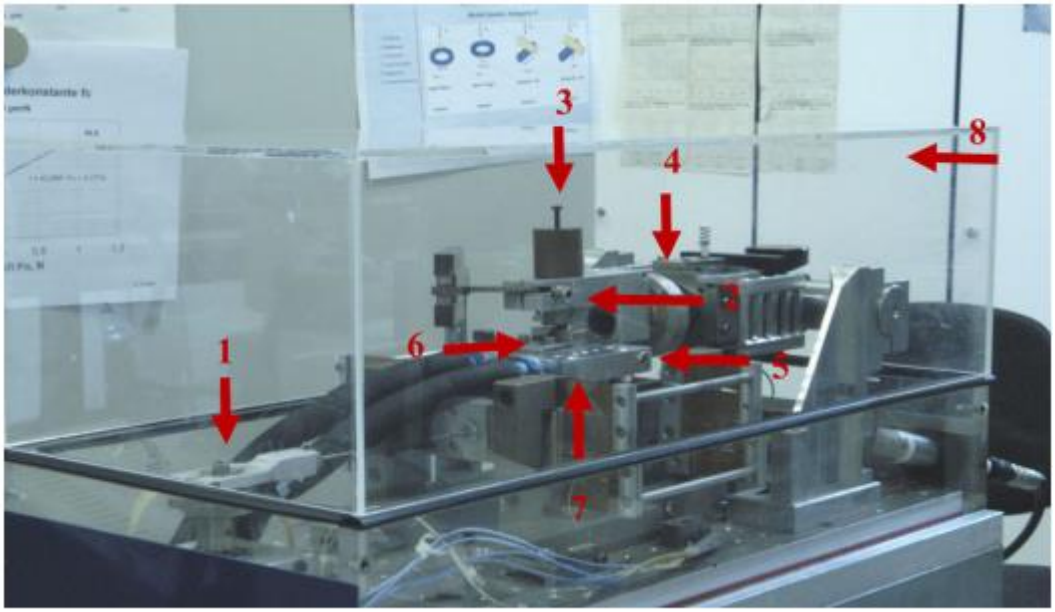

Figure 3.6. Photograph of the reciprocating sliding tribometer. 1. D.C motor with eccentric adjustment, 2. top arm with integrated load cell, 3. dead weight, 4. rotational arm, 5. vibrating table, 6. steel disk holding unit, 7. heating element and thermocouple holding unit, and 8. Plexiglas chamber (Reprinted with permission from reference [3]).

3.6.2. Multifunctional tribometer (MFT).

A multifunctional tribometer supplied by RTEC instruments was used for reciprocating testing of PU-based coatings. The tribometer operates at ambient temperature in the load range of 10-40 N, the frequency range of 0-15 Hz, and the stroke length of 0-5 mm. The reciprocating table in this tribometer was controlled with a servo motor.

3.6.3. Nanoscratch tester and nanotribometer.

The UMT-2, CETR (Bruker) nanoscratch tester/ nanotribometer has nanoscratch testing and reciprocating tribotesting modules. The nanoscratch testing module was used to calculate the adhesive strength of the coating with the substrate. It was equipped with an acoustic emission

detector, which detects fluctuations in acoustic signals arising from failure and breaking of the coating. It had a spherical diamond tip indenter of 5 and 200 µm sizes, operating in the load range of 50 mN to 50 N. The nanotribometer module was equipped with a 4 mm spherical tungsten carbide indenter, operating in the load range of 0-10 N, with frequency and stroke length up to 5 Hz and 75 mm, respectively.

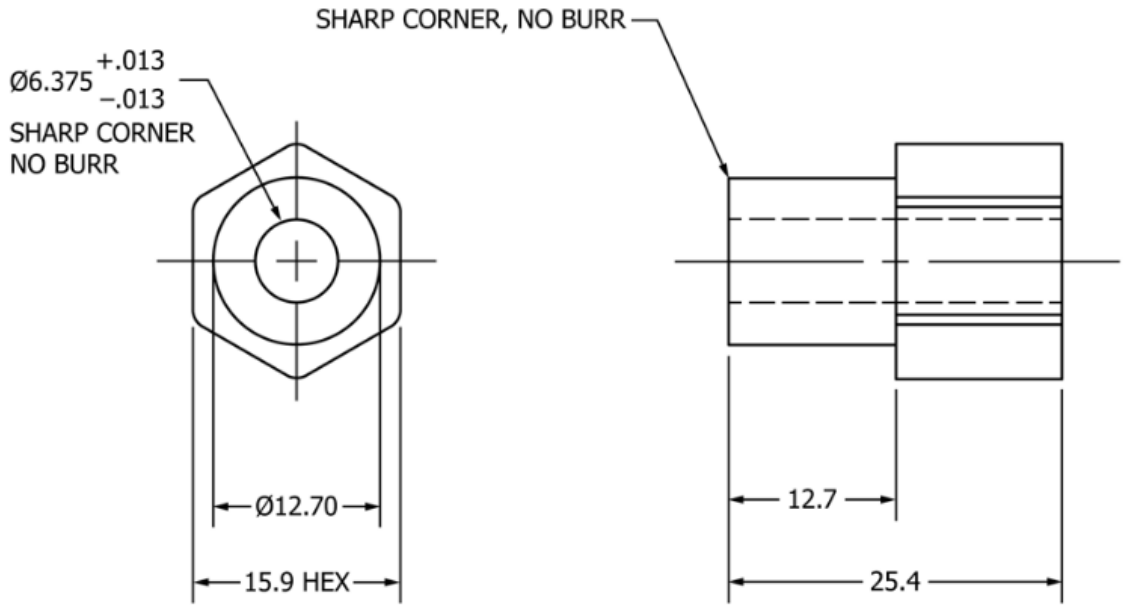

Figure 3.7. Schematics of test samples (Reprinted with permission from reference [7])

3.6.4. Galling tester.

The test apparatus was developed to adhere to ASTM G196 (schematics of test specimen shown in **Figure 3.7**), which requires the use of two hollow, concentric cylindrical specimens with their ends mated to provide an annular area of contact. An alignment pin is placed between the top and bottom specimens to achieve appropriate alignment and concentricity between the mating specimens. One specimen is kept stationary while the other is rotated about its axis. **Figure 3.8** shows the schematic representation of the galling test apparatus. The specimen is placed on the specimen holder, which is mounted at the bottom and rotates in a clockwise direction. A speed reduction gearbox (1:150) and an AC motor with a spindle speed of 1350 rpm are used to operate the spindle. Radial encoders are used to measure rotational speed,

whereas AC drives are used to control motor speed. The top specimen is fitted using spring pressure after being inserted into a holder with flat sides. Pneumatic bellows apply the load to the top specimen, ensuring consistent loading even when the specimen deforms quickly. An axial load cell positioned at the base of the pneumatic bellows measures the compressive load between the specimens. The test apparatus can apply loads up to 2000 N. The bottom specimen is rotated at a speed of 6 rpm after the appropriate load has been applied to the top specimen. The load cell, which is mounted over the base plate at a distance of 100mm, measures the frictional force. During the test, the data related to axial compressive load and frictional torque are acquired online in the LABVIEW software in the computer attached to the test rig. The galling is observed from the rapid fluctuations in frictional torque data.

The test equipment also has been set up to conduct experiments at temperatures as high as 400˚C. A coil heater is used during testing to heat the top and bottom specimens while they are assembled. The specimens are heated uniformly due to the coil heater housing configuration. The coil heater assembly uses two temperature sensors (J and K-type thermocouples). The J-type thermocouple is installed along with the heater element to prevent the heater temperature from rising above the predetermined level. The sensor tip of a K-type thermocouple is put through the heater housing until it reaches the top specimen.

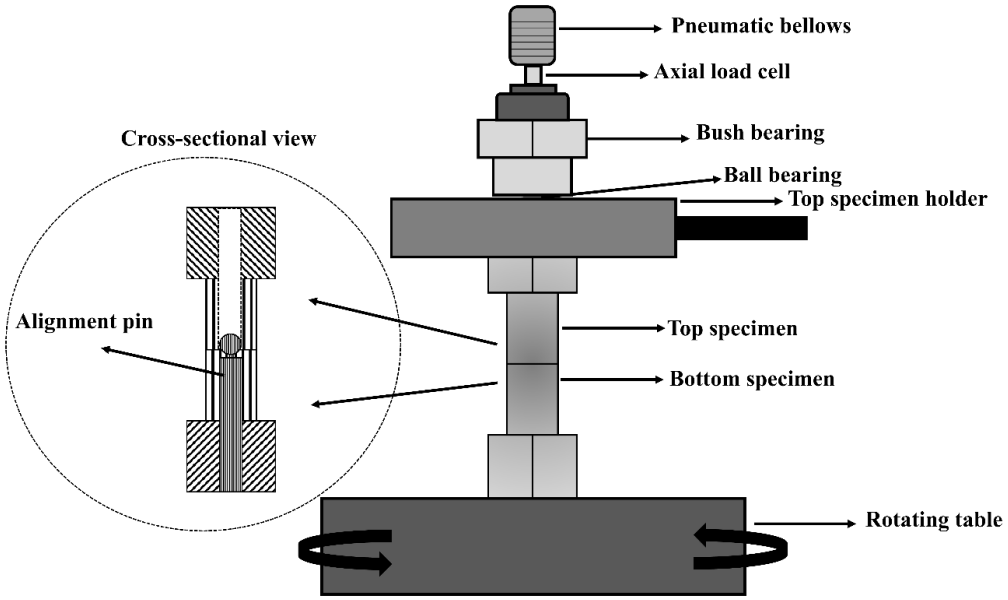

Figure 3.8. Schematic representation of the galling test apparatus.

3.7. Summary.

The chapter discusses the procedure of developing MoS_2 nanosheets. Also, the detailed discussion of instruments used for coating, tribological testing, and their characterization has been explained. The inputs given to these testing instruments varied for different coatings and are provided in the later chapters. Since all the three coatings to be studied in this present study are unique, the test parameters and analysis techniques used for them were also different. All those test parameters and analysis techniques will be found in the later chapters of the associated coatings.